

Low resolution electromagnetic tomography: a new method for localizing electrical activity in the brain

R.D. Pascual-Marqui^{a,b}, C.M. Michel^{a,*}, D. Lehmann^b

^a *Functional Brain Mapping Laboratory, Department of Neurology, University Hospital, HCUG, CH-1211 Geneva, Switzerland*

^b *EEG / EP Mapping Laboratory, Department of Neurology, University Hospital, CH-8091 Zurich, Switzerland*

Received 16 July 1994; accepted 19 August 1994

Abstract

This paper presents a new method for localizing the electric activity in the brain based on multichannel surface EEG recordings. In contrast to the models presented up to now the new method does not assume a limited number of dipolar point sources nor a distribution on a given known surface, but directly computes a current distribution throughout the full brain volume. In order to find a unique solution for the 3-dimensional distribution among the infinite set of different possible solutions, the method assumes that neighboring neurons are simultaneously and synchronously activated. This basic assumption rests on evidence from single cell recordings in the brain that demonstrates strong synchronization of adjacent neurons. In view of this physiological consideration the computational task is to select the smoothest of all possible 3-dimensional current distributions, a task that is a common procedure in generalized signal processing. The result is a true 3-dimensional tomography with the characteristic that localization is preserved with a certain amount of dispersion, i.e., it has a relatively low spatial resolution. The new method, which we call Low Resolution Electromagnetic Tomography (LORETA) is illustrated with two different sets of evoked potential data, the first showing the tomography of the P100 component to checkerboard stimulation of the left, right, upper and lower hemiretina, and the second showing the results for the auditory N100 component and the two cognitive components CNV and P300. A direct comparison of the tomography results with those obtained from fitting one and two dipoles illustrates that the new method provides physiologically meaningful results while dipolar solutions fail in many situations. In the case of the cognitive components, the method offers new hypotheses on the location of higher cognitive functions in the brain.

Keywords: Brain mapping; 3D distributed source localization; Brain activity tomography; Visual evoked potentials; Auditory evoked potentials; Cognitive event related potentials

1. Introduction

The question of localizing electrical sources in the brain from surface recordings (electric or

magnetic) has attracted the EEG/MEG community for some time now (Fender, 1987; Williamson and Kaufman, 1987; Wikswo et al., 1993). Most attempts are based on equivalent dipole computations (Henderson et al., 1975; Kavanagh et al., 1978) where single or multiple point sources in the brain are estimated from the measured elec-

* Corresponding author. E-mail: christo@cih.hcuge.ch

tric or magnetic potential fields using spherical or (more recently) real head shape models (Hämäläinen and Sarvas, 1989). While the general forward solution is well-defined (i.e., a given source configuration generates a particular electric and magnetic field), the inverse solution is ambiguous (i.e., there is an infinite number of different source configurations that can explain a measured electric and/or magnetic field). There is no unique solution to this inverse problem with the models presented up to now, e.g. there is no way to determine the true number of point sources that were simultaneously active in the multiple dipole model, or, more in general, to determine whatever arbitrary form of activity distribution existed. Thus, a general 3-dimensional (3D) imaging throughout the brain, i.e., a tomography based on the electric-magnetic fields has not yet been presented. New localization models such as those based on the minimum norm approach (Ioannides et al., 1990; Wang et al., 1992) or those utilizing temporal information and introducing spatio-temporal constraints (Scherg and Berg, 1991) do not overcome this basic difficulty, since the solutions are still not truly 3D (Wikswow et al., 1993; Ilmoniemi, 1993).

The novel approach that we present in this paper is based on the idea to find a direct 3D solution of the electric activity distribution. Only such a solution can be called a "tomography" in the same sense that it is known from radiological procedures such as PET, MRI or CT. The way to obtain a meaningful 3D solution despite the curse of non-uniqueness is by sacrificing spatial resolution. Instead of estimating point dipoles we compute distributed activity throughout the brain volume, which is discretized as a dense 3D grid where electric sources are located on each grid point. The strength and direction of the activity at each of these grid points determine the electric and magnetic field that can be measured on the scalp. The crucial question is to find a general purpose meaningful solution among the infinite set of different solutions that lead to the same measured surface fields.

From a physiological point of view, the solution must take into account that neighboring neurons are most likely to be active synchronously

and simultaneously. Synchronization has been demonstrated in a number of animal studies where oscillatory and coherent activity of closely spaced neurons was intracranially recorded with multi-electrode arrays. Temporal coherence of spatially adjacent neurons has been demonstrated in the spontaneously active and in the stimulated brain, in different areas of the visual, somatosensory and motor cortex, for different temporal frequencies (Andersen and Andersson, 1968; Bland, 1986; Llinas, 1988; Gray et al., 1989; Eckhorn et al., 1989; Engel et al., 1990; Silva et al., 1991). States of synchrony produced by oscillating neurons over small distances have been described (Steriade et al., 1990; Murthy and Fetz, 1991). Oscillatory neuronal responses in general have recently been reviewed at length by Kreiter and Singer (1992) and by Bland and Colom (1993). From a functional point of view both reviews suggest that such synchronization of neuronal structures could serve "as a basic binding mechanism to establish relations between distributed neuronal responses" (Kreiter and Singer, 1992, page 374) and "entraining them into a common processing mode and tuning them selectively for the reception of particular kinds of information flow" (Bland and Colom, 1993, page 201).

This physiological consideration can be used in our model by assuming that neighboring grid points are more likely to be synchronized (i.e., of similar orientation and strength) than grid points that are far from each other. In mathematical terms, the task is to find the smoothest of all possible solutions. Maximizing smoothness is a common procedure in generalized signal processing (Titterton, 1985) and can be applied here to find a unique, optimal and physiological meaningful 3D distribution of electrical activity in the brain. The characteristic feature of this solution is its relatively low spatial resolution, which is a direct consequence of the smoothness constraint. Specifically, the solution produces a "blurred-localized" image of a point source, conserving the location of maximal activity, but with a certain degree of dispersion. It should be emphasized that this solution will also produce a "blurred-localized" image of any arbitrary distribution, due to the principle of superposition. In practical

terms, this means that we can produce a low resolution tomography of the electrical activity at every moment in time with the advantage of the time resolution of the electric-magnetic recordings. We call this method Low Resolution Electromagnetic Tomography and abbreviate it with the acronym "LORETA".

2. Methods

We will present the new method with simulated examples and with two sets of real data from several subjects. The first set of data are 21-channel visual evoked potentials to checkerboard stimulation of the upper, lower, left and right hemiretina. Here we examined the tomography of the P100 component. The second set of data are 47-channel event related potentials in a paradigm where auditory warning stimuli were followed by visual stimuli that were either targets or non-targets. From these data we analyzed the auditory N100 component and the two cognitive components CNV and P300.

Simulation

As simulation examples we selected 2 radially oriented point sources (dipoles) in the brain and computed the 21 channel forward solution electric potential map using a 3-shell unit radius spherical head model (Ary et al., 1981). The 2 dipoles were located 2.5 cm (head radius: 7.8 cm) above the T3-T4-Oz plane in the left hemisphere (eccentricity: 5.1 cm). In two examples considered here the anterior-posterior distance between the pair of dipoles was 1.5 and 3.1 cm. The forward solution maps were then used as input for the LORETA computation in order to test the location precision and the ability of the method to separate the two known dipole locations.

Visual evoked potentials

Data from 21 subjects (11 women, 10 men, mean age: 26 years) were examined with 21-channel evoked potential recordings during checkerboard stimulation. The subjects viewed a translucent circular screen of 15.5 deg arc from a distance of 90 cm, onto which a black and white

checkerboard pattern with 55 min arc checks was projected. The subject positioned his head into a chin-forehead-rest and fixated a black triangle of 20 min arc at the upper, lower, right or left edge of the stimulus field. Seventy checkerboard reversal stimuli were presented at a rate of 1.1/s using a feedback controlled mirror galvanometer system with 50 cs/m² mean luminance, 94% contrast and less than 0.5 ms reversal time. The electric signals were collected with a BioLogic Brain Atlas System and averaged on-line using a software artifact rejection window. The electrode position array extended 60% of theinion-nasion arc (starting at inion), and covered 80% of the distance between the two pre-auricular points. The most anterior electrode on the midline was used as recording reference and the data were off-line recomputed against the average reference. The data were analyzed in previous papers in terms of spatial characteristics and instantaneous frequencies (Capaul, 1990; Witte et al., 1992).

From the grand mean average evoked potential maps of all subjects we selected the point of maximal Global Field Power (GFP) in the time segment between 80 and 130 ms, corresponding to the visual P100 component. GFP is the spatial standard deviation of the average reference potential map at each moment in time, indicating the instantaneous strength of the field (Lehmann and Skrandies, 1980).

Auditory-visual event related potentials

These data were taken from a drug study with 10 healthy, right-handed male volunteers (mean age 26.7 years). In this study different types of event related potentials (ERP) and spontaneous EEG were recorded. Each subject participated in four sessions in intervals of 1 week. In the 4 sessions they received, in a double-blind cross-over design, one of 3 different doses of piracetam or placebo. For this paper we selected only one ERP task and averaged the data of all 4 sessions, independent of the drug intake. The selected task consisted of repetitive presentation of a pair of auditory and visual stimuli. The interval between the stimulus pair was fixed to 704 ms while the

interval between pairs was randomized between 704 ms and 2.4 s. The auditory stimulus served as the warning stimulus and was always a 2000 Hz tone of 55 ms duration and 80 dB loudness presented through a loudspeaker that was positioned 1 m in front of the subjects (above the monitor). The following visual imperative stimulus was either a black cross or a black square of 6.9 deg arc on white background viewed from a distance of 1 m. It was presented for 100 ms and the subject's task was to press with his right hand a mouse button as fast as possible only after the presentation of a cross. Crosses (targets) were presented randomly with a probability of 33%. Around 30 targets and 60 non-targets were presented within a 3 min trial.

Forty-seven electrodes were placed with regular spacing on a grid extending from 20% of the nasion-inion distance to the inion and from 10% above the left to 10% above the right pre-auricular point. The number of electrodes per row (from left to right) was 3, 5, 5, 7, 7, 7, 5, 5, 3. The EEG signals were collected continuously throughout a complete trial with a 64-channel amplifier system (M&I, Prague, Czech Republic), an A/D-converter by Burr Brown and an acquisition software by Neuroscience Technology Research (Prague, Czech Republic). Data were converted at 1024 Hz per channel and stored in memory on a 486/50 MHz PC. After the end of each recording, the data were written on hard disk after down-sampling them to 256 Hz. Analog filter settings were at 0.1–40 Hz.

Only the brain electric response to targets was used in this analysis. The data was projected linearly onto a regular-spaced 21-channel grid according to the 10–20 system. These ERP data were then averaged over subjects and 3 particular time points of maximal GFP were selected from the map series: between 80 and 130 ms after the auditory stimulus (corresponding to the auditory N100 component), between 500 and 700 ms before the onset of the imperative stimulus (representing the period of the Contingent Negative Variation, CNV), and between 900 and 1100 ms (which means between 200 and 400 ms after the imperative stimulus) corresponding to the P300 component.

LORETA and dipole computations

For the LORETA computation we assumed a 3-shell spherical head model with a radius of 78 mm and equal inter-electrode distances on the scalp. Electrical brain activity was calculated on a regular 3D grid consisting of 1153 points, lying within the upper hemisphere, with a radius equal to 86% of the total sphere radius (corresponding to the outer cortex). The minimum inter-point distance was 8.385 mm. All computations were performed on a 486/50 MHz PC. The complete mathematical formulation is given in the Appendix. Computation time to determine the linear transfer matrix for the inverse solution was around 1 hour and had to be performed only once for a given electrode array. In addition to the LORETA computation, one and two equivalent dipoles were fitted into the same electric field maps. The same 3-shell spherical head model was used for dipole fitting.

3. Results

The results of the LORETA computations are shown in the figures that follow as top-view horizontal slices through the brain at 8 different depths, with inter-slice distance of 8.385 mm. The deepest slice (0 cm) corresponds to the T3-T4-Oz plane. Besides the LORETA results, the electric potential maps and the solution of the one and two dipole computations are displayed. In the real data cases, the GFP and the selected time point are also shown.

Simulation

The simulated examples with two closely spaced dipoles illustrate the spatial resolution capability of LORETA. Based on the potential field generated by dipoles that were located 1.5 cm apart, LORETA produced a 3D blurred area that covered the location of both point sources (Fig. 1). When they were 3.1 cm apart, LORETA was able to separate them clearly with two blurred areas on the left side (Fig. 2), illustrating what we call low resolution. An additional illustration is given by fitting one point source to the potential maps. The best fitting single dipole was located at

the midpoint between the two actual dipoles in both examples. Even though these solutions were incorrect, they explained the maps very well (100% explained variance for dipoles 1.5 cm apart, and 99.6% explained variance for dipoles 3.1 cm apart).

Visual evoked potentials

Figs. 3 to 6 show the GFP, the selected potential map, the equivalent dipole locations, and the LORETA images of the P100 component for the four fixation conditions during checkerboard reversal stimulation. Figs. 3 and 4 correspond to left and right hemiretina stimulation, respectively. The two GFP traces are nearly identical,

showing 3 dominant peaks at 70, 100 and 140 ms. The maps at 100 ms show clearly lateralized topography. The single equivalent dipole at the 100 ms peak was located slightly to the left for left hemiretina (right hemifield) stimulation, and to the right for right hemiretina (left hemifield) stimulation. The LORETA images also show dominant electrical activity ipsilateral to the stimulated hemiretina with maximal activity at the outermost occipital border of the second and third slices (8.38-16.77 mm above the zero plane). From a qualitative point of view there is a fair agreement between the locations obtained from LORETA and from the single equivalent dipole. The LORETA solutions, however, show that

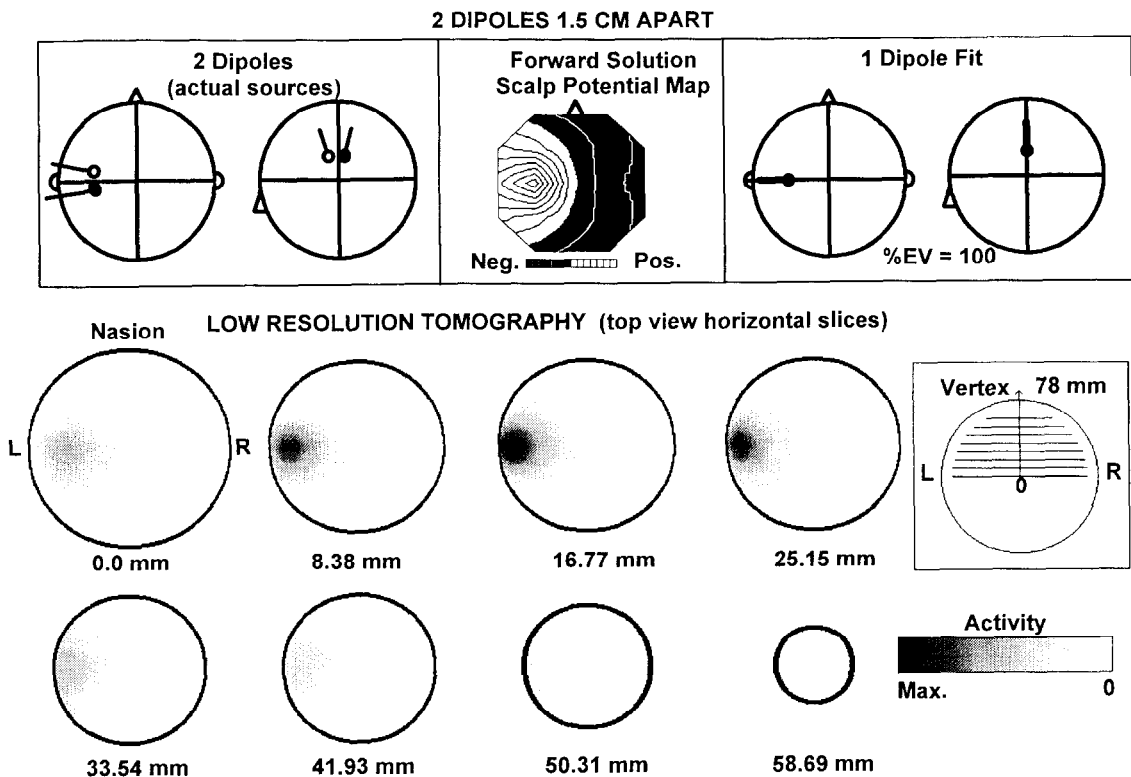


Fig. 1. Low resolution brain electromagnetic tomographic (LORETA) images depicting the estimated current density strength corresponding to an actual current density consisting of two point sources 1.5 cm apart in a 7.8 cm radius head (top-left inset). Estimation is based on the forward solution electric potential map shown in the top-center inset. The top-right inset shows the best fitting single dipole to the map, which explains 100% of the variance (%EV), but lies between the actual point sources. The tomographic images are parallel horizontal brain slices viewed from the top of the head, with the indicated orientation (L: left, R: right). The middle-right inset illustrates in a posterior head view the height of each brain slice. The LORETA images do not resolve the two point sources, producing a single blurred region with maximum activity containing both generators.

there is also contralateral activity even though it is weaker than the ipsilateral, indicating a remarkable contralateral synchronous activation of neurons 100 ms after visual stimulation.

Figs. 5 and 6 show the results for upper and lower hemiretina stimulation. The GFP curves are dominated by one peak at around 100 ms. The GFP was however larger and the peak latency was earlier for upper hemiretina as compared to lower hemiretina stimulation. The single equivalent dipole for these electric fields were located on the midline, with upward orientation for upper hemiretina and downward orientation for lower hemiretina stimulation. No difference in the inferior-superior location of the single dipoles was found. Two best-fitting dipoles did not show any tendency to be located in the two

visual cortices, even though they explained more than 98% of the variance. They were both located in the right occipital area for upper hemiretina stimulation, and in the middle occipital and deep right parietal areas for the lower hemiretina stimulation, respectively. On the other hand, the LORETA images produced for both conditions similar activation of the right and left occipital areas, as expected. Activation was stronger for upper than for lower hemiretina. In addition, the location of the active area for upper hemiretina stimulation was superior (in height) compared to that of the lower hemiretina stimulation, as can be more clearly appreciated from the ratios of maximum activity of the second slice (8.38 mm) to the first slice (0 mm), which were 1.01 for upper and 0.89 for lower hemiretina stimulation.

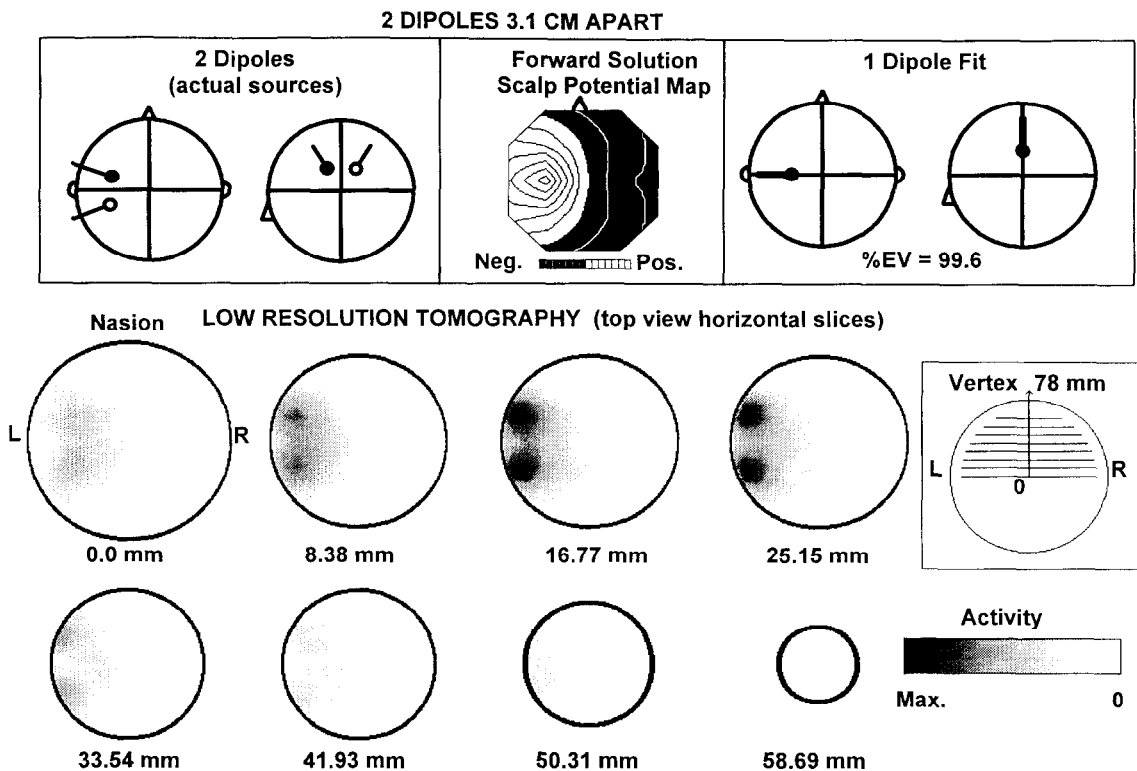


Fig. 2. Low resolution brain electromagnetic tomographic (LORETA) images shown with the same conventions as in Fig. 1. In this case the actual current density consists of two point sources 3.1 cm apart. The best fitting single dipole explains 99.6% of the variance, but is again located between the actual point sources. The LORETA images now resolve the sources, producing two regions of high activity density, each containing one of the generators.

Auditory-visual event related potentials

Figures 7–10 show the activity distribution results for different time points of the ERP in the auditory-visual CNV paradigm. Fig. 7 corresponds to the first dominant GFP peak 94 ms after the onset of the auditory warning stimulus. The electric field map shows the typical auditory N100 component pattern. Fitting a single dipole to this map resulted in a meaningless location in the middle of the brain. The two equivalent dipoles were also not at all located in the areas of the auditory cortices, but were found in central and occipital midline locations. LORETA however clearly localized two dominant active areas in the left and right temporal lobes.

The next selected time point was during the sustained CNV between the two stimuli (Fig. 8). The single dipole solution was again located nearly in the center of the head. Fitting two equivalent dipoles resulted in one deep frontal dipole and the other one superficial occipital, explaining 99.6% of the measured field. The LORETA computation resulted in superficial frontal lateral activity in both hemispheres.

The last selected time point was at the GFP peak of the strong P300 component after the target stimulus (Fig. 9). The map configuration showed the well-known central positivity. The single dipole solution was located under this central positivity and pointing towards it. The two-di-

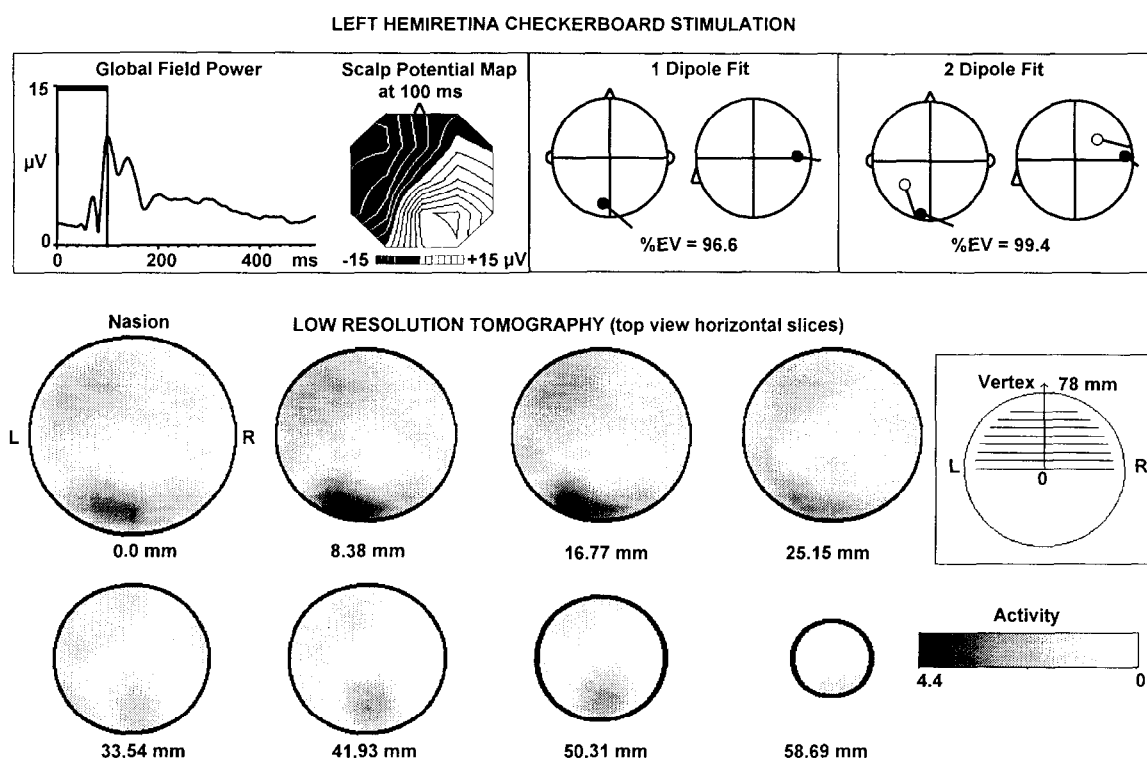


Fig. 3. Low resolution brain electromagnetic tomographic (LORETA) images depicting the estimated current density strength corresponding to the P100 response to left hemiretina checkerboard stimulation. The top-left inset illustrates the Global Field Power curve with the P100 peak marked therein, and its electric potential map. The top-center inset shows the best fitting single dipole to the map (96.6% explained variance, %EV), and the top-right inset shows the best fitting two-dipole model (99.6% explained variance, %EV). The tomographic images are parallel horizontal brain slices viewed from the top of the head, with the indicated orientation (L: left, R: right). The middle-right inset illustrates in a posterior head view the height of each brain slice. The single best fitting dipole location is slightly left lateralized in the occipital cortex. LORETA images indicate major activity in the left occipital cortex, but also shows some contralateral weaker activity.

pole solution explained 99.8% of the variance and were located in frontal and parietal areas respectively. The LORETA solution however showed a superficial widely blurred left frontal activity, going over all first four slices.

4. Discussion

The main goal of this paper was to demonstrate with examples a novel method for localizing non-ambiguously the electrical activity in the brain from the recorded electric field on the surface.

The simulations of electric potential field maps generated from dipoles represent the most severe test for our method, because they constitute the “non-smoothest” possible current density. Despite this fact, the method correctly localized the

two point sources; though, due to the inherent characteristics of the method, the solutions were blurred-localized images of the point sources. Thus, if brain activity has the property of being dipolar, then our method would result in worse spatial resolution than equivalent dipole computations. However, it is generally not known a priori if the sources are point like, and even less how many of them are active. A single dipole solution in these examples based on two dipoles explained over 99.6% of the variance, but was incorrectly located between the two actual sources. LORETA, nevertheless, at least separated the two sources when they were 3.1 cm apart. Consequently, without any a priori knowledge the method was able to localize the two sources with the dominant activity being located exactly where the dipoles were placed.

The simulation examples constructed in Figs. 1

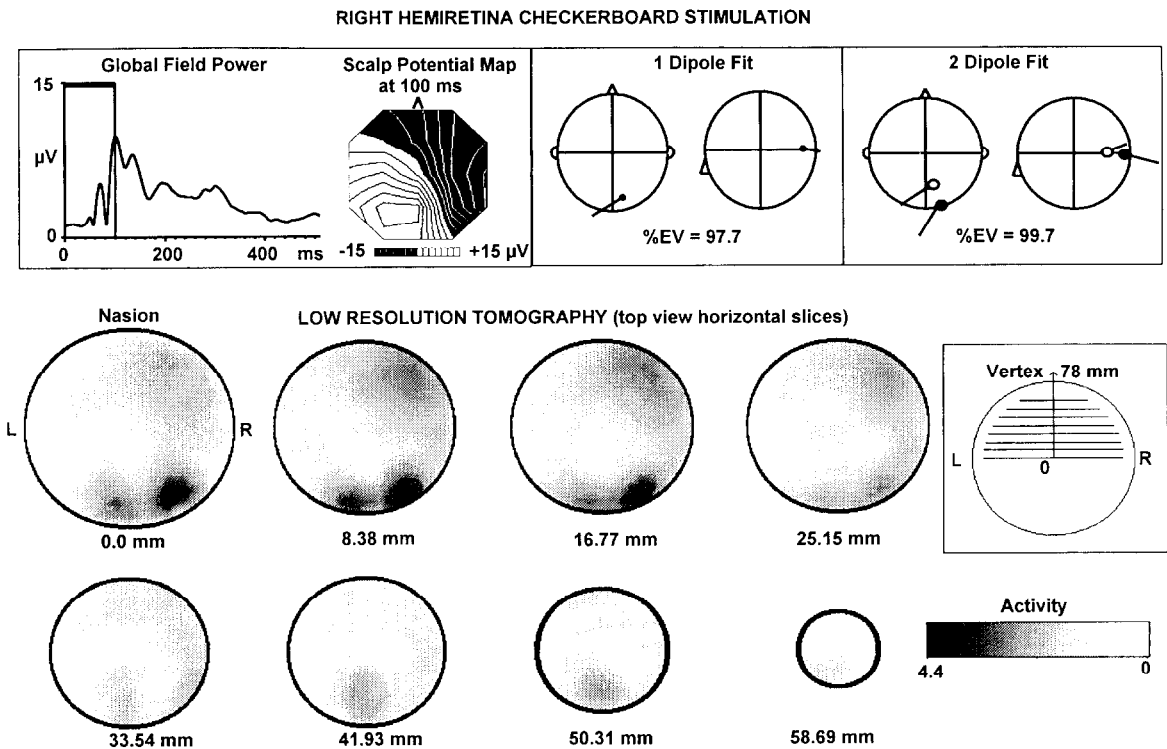


Fig. 4. Low resolution brain electromagnetic tomographic (LORETA) images (shown with the same conventions as in Fig. 3) corresponding to the P100 response to right hemiretina checkerboard stimulation. The single best fitting dipole location is slightly right lateralized in the occipital cortex. LORETA images indicate major activity in the right occipital cortex, but again shows some contralateral weaker activity.

and 2 contain implicitly a completely different simulation experiment. If the actual current density were smoothly distributed in 3D space, e.g. if it were identical to the LORETA solution obtained from the dipole sources, then the new estimated LORETA solution would be exactly itself again. This trivial and self-supporting fact points to the notion that smooth current densities can be precisely estimated by the new tomography.

The non-uniqueness of the solution to the 3D inverse problem has always been identified with the impossibility of localizing brain activity without any a priori knowledge about the brain activity. The general view, as can be seen from the literature (see Wikswa et al., 1993, for a review and references therein), is that this constitutes an

insurmountable difficulty, due to a fundamental physical limitation imposed by nature. The main reason for such an unfortunate state of affairs is that the measurements contain insufficient information. The new method presented here gives a fairly satisfactory solution to this problem. It is based on a new important finding: the measurements contain *sufficient* information for the *approximate* determination of the full 3D source distribution, without needing any a priori knowledge about what we precisely want to know about. *Approximate* means, e.g., that a point source will be resolved in a blurred form, and there is no way to distinguish if the actual source was point-like or blurred.

The results of the checkerboard evoked potential fields demonstrated that the new method

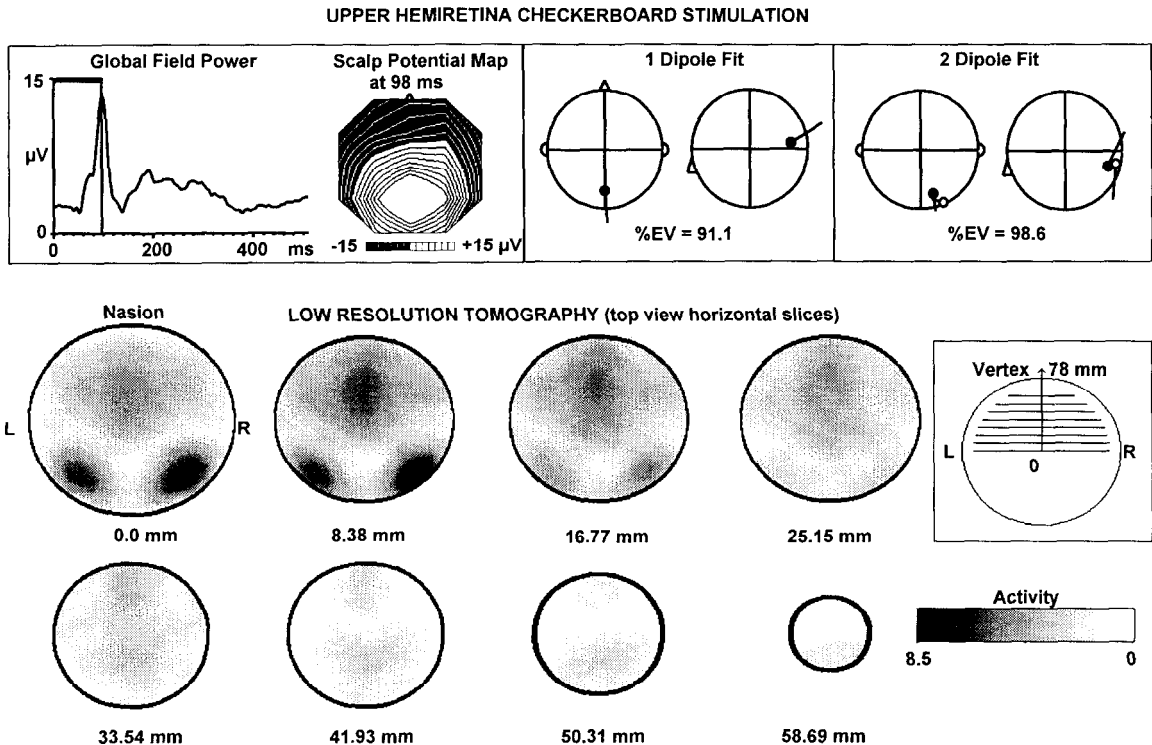


Fig. 5. Low resolution brain electromagnetic tomographic (LORETA) images (shown with the same conventions as in Fig. 3) corresponding to the P100 response to upper hemiretina checkerboard stimulation. The single best fitting dipole explains 91.1% of the variance, but is located in the midline occipital area with upward orientation. The two best fitting dipoles do not show any tendency to be located in the two visual cortices, even though they explain 98.6% of the variance. LORETA images produce similar activation of the right and left occipital areas. The ratio of maximum activity of the second slice (8.38 mm) to the first slice (0 mm) is 1.01.

generates physiologically meaningful results without any a priori constraints. Left and right hemiretina stimulation resulted in dominant left and right hemisphere activity, respectively. Single dipole computations also showed this lateralization of the P100 component. Both methods are in fair qualitative agreement showing ipsilateral electric activity 100 ms after unilateral hemiretina stimulation, as has been described earlier with brain mapping (Barrett et al., 1976; Witte et al., 1992), dipole fitting (Darcey et al., 1980) and intracranial recordings (Lehmann et al., 1982). However, our new method found also considerable activity contralateral to the stimulated hemiretina, a result that can of course not be seen with one dipole solution, and that was also not

found with two dipole fits. This contralateral activity 100 ms after unilateral stimulation is well explained by inter-hemispheric transfer through the corpus callosum (Brown et al., 1994) that is known to take place much earlier than 100 ms via inter-hemispheric connections between visual areas 18 (Harvey, 1980; Grüsser and Landis, 1991). Concerning the upper vs. lower hemiretina stimulation, we expected earlier, stronger and more superiorly located activity for former case, with bilateral occipital activity under both conditions (Lehmann and Skrandies, 1979; Skrandies et al., 1980; Lehmann et al., 1982; Skrandies, 1987). Our data showed indeed an earlier peak latency and stronger GFP for upper than lower hemiretina stimulation. Statistical analysis of the

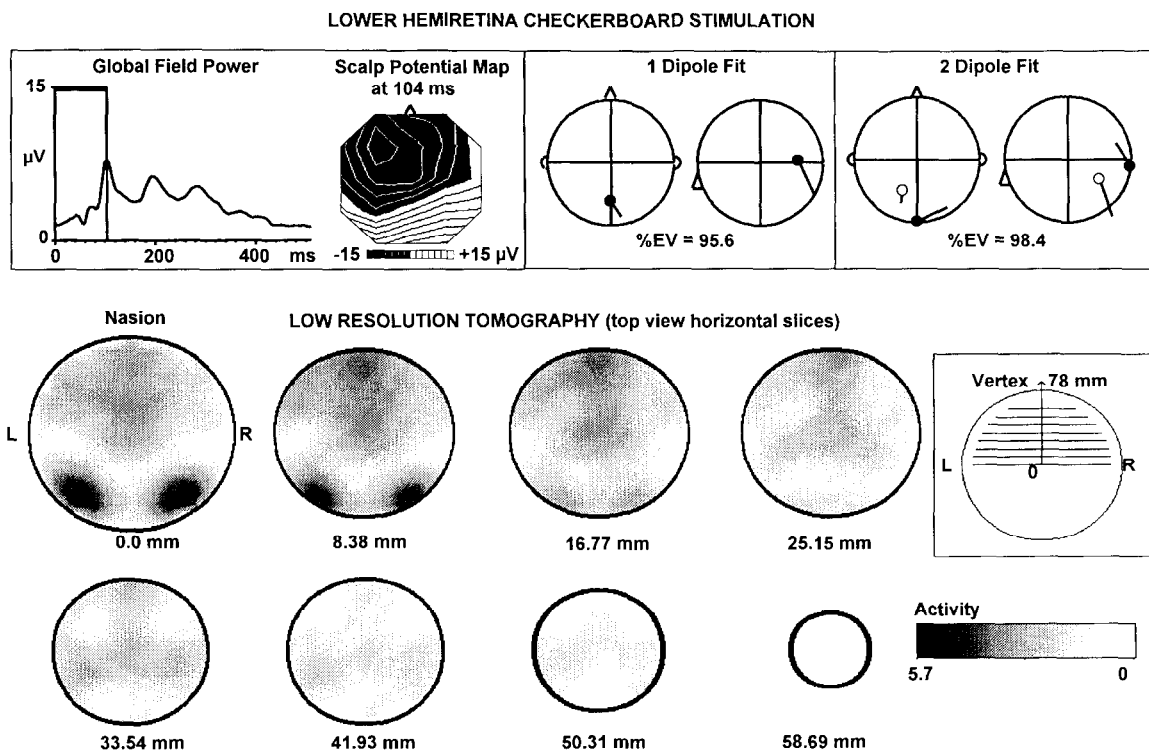


Fig. 6. Low resolution brain electromagnetic tomographic (LORETA) images (shown with the same conventions as in Fig. 3) corresponding to the P100 response to lower hemiretina checkerboard stimulation. The single best fitting dipole explains 95.6% of the variance and is located in the midline occipital area with downward orientation. The two best fitting dipoles do not show any tendency to be located in the two visual cortices, even though they explain 98.4% of the variance. LORETA images produce similar activation of the right and left occipital areas. The ratio of maximum activity of the second slice (8.38 mm) to the first slice (0 mm) is 0.89, indicating an inferior location as compared to upper hemiretina stimulation (Fig. 5). Note also the different activity scale as compared to Fig. 5, indicating weaker activity for lower than for upper hemiretina stimulation.

data over subjects showed that these differences were significant (Capaul, 1990). In terms of location of the activity, neither one nor two dipole computations resulted in more superior dipole positions for upper than for lower hemiretina stimulation. In addition, fitting two dipoles did not result in locations in the two hemispheres for either condition. On the other hand, the LORETA result clearly showed bilateral occipital activity in both conditions, and it also showed the expected more superior activity location for upper as compared to lower hemiretina stimulation.

The analysis of the auditory N100 component in the second data set clearly illustrated the advantage of the new localization method as com-

pared to equivalent dipole solutions. The two-dipole fit (explaining 99.9% of the variance) produced locations in the middle of the head instead of the expected temporal lobes (Williamson and Kaufman, 1987; Pantev et al., 1988). And of course the single dipole location did not make sense in view of the well known two active areas for the N100 component. However, the LORETA computation resulted in dominant activation of the left and right temporal cortical areas, in the region of the auditory cortices. This result shows that the new method is able to correctly localize the late auditory component of the electric recordings without introducing the a priori constraints that were repeatedly suggested by Scherg

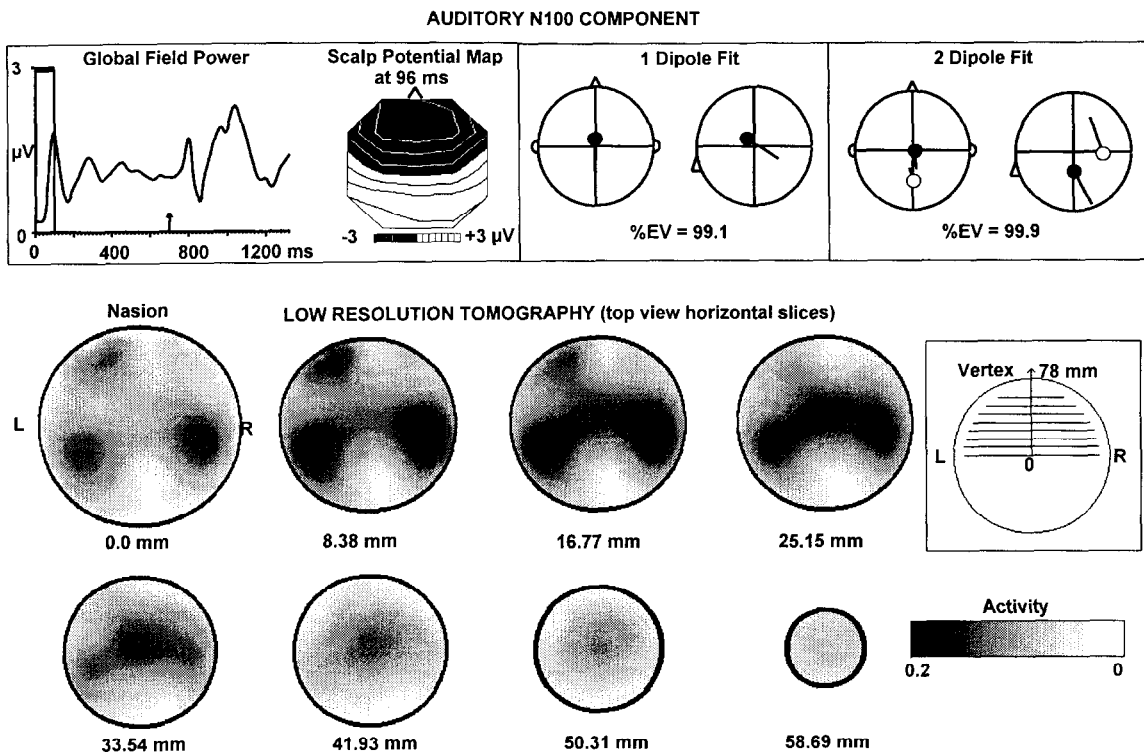


Fig. 7. Low resolution brain electromagnetic tomographic (LORETA) images depicting the estimated current density strength corresponding to the auditory N100 response in an auditory-visual CNV-paradigm. The top-left inset illustrates the Global Field Power with the indicated peak at 94 ms after the onset of the auditory warning stimulus, and its electric potential map. The small arrow at 704 ms marks the onset of the visual target stimulus. The top-center inset shows the best fitting single dipole to the map, and the top-right inset shows the best fitting two-dipole model. The tomographic images are parallel horizontal brain slices viewed from the top of the head, with the indicated orientation (L: left, R: right). The middle-right inset illustrates in a posterior head view the height of each brain slice. The single best fitting dipole explains 99.1% of the variance, but is located in the middle of the head. The two best fitting dipoles do not show any tendency to be located in the two auditory cortices, even though they explain 99.9% of the variance. LORETA images produce similar activation of the right and left auditory cortical areas.

et al. (1989). The location precision of LORETA was in this case limited by the stimulation procedure with a simple loudspeaker instead of earphones. A proper examination of the N100 location would need a more adequate experimental design.

In the case of the cognitive ERP components, where no consistent findings about the active areas are available, our method provides new suggestions about brain regions that are involved during preparation (CNV) and in decision making (P300). In both cases no obvious correspondences between the equivalent dipole solutions and the LORETA solutions were found. The new method suggests bilateral symmetric fronto-temporal sources for the CNV, a result that is partly supported by a recent MEG study of Elbert et al. (1994), who suggested an overlap of frontal and temporal sources for the early component of the CNV. These authors showed in addition that a

single equivalent dipole model is not satisfactory for explaining the CNV which is assumed to consist of distributed sources in different cortical areas. Our new method is able to differentiate such multiple active areas. As for the P300, little is known about the possible generators. Hippocampal sources (Okada et al., 1983; O'Connor and Starr, 1985; Başar-Eroglu et al., 1991) as well as several different cortical generator sites (Kiss et al., 1989; Ford et al., 1993; Johnson, 1993; Trahms et al., 1993) have been suggested. Our data suggest a dominant left frontal cortical activity at peak time of the P300 component in a task where right button press was asked from the subjects. Whether or not this lateralized activity is due to (unilateral) eye blinks or whether it was related to the site of the motoric response has to be verified in further experiments.

The results presented in this paper should be considered as a first demonstration of the capa-

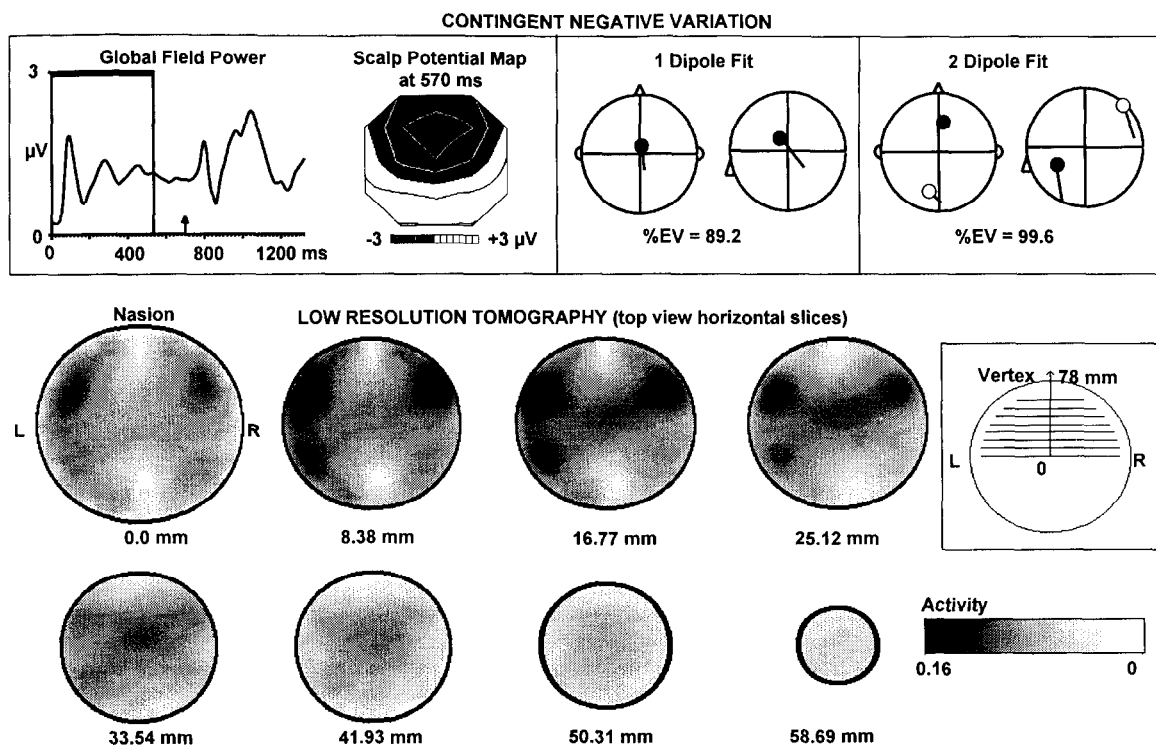


Fig. 8. Low resolution brain electromagnetic tomographic (LORETA) images (shown with the same conventions as in Fig. 7) corresponding to the sustained CNV between the two stimuli. The LORETA images suggest superficial frontal lateral activity in both hemispheres, a result that is not obvious from the one and two dipole source models.

bility of the new method to localize electric sources in the brain. Many points have to be further developed before applications of the method can be considered. It is clear that the spatial resolution has to be increased. The term low resolution is necessary for the data presented here. However, we are convinced that the resolution can be improved with better recording and analysis techniques:

First of all, sufficient electrodes adequately covering the maximum possible brain area are needed. In the first example, the 21 electrodes covered only the pre-central to occipital area. No information about frontal activity was therefore available. In the second data set there were 47-channels which had to be down-sampled to 21 channels due to the high sensitivity of the method to deviations from the spherical head model which becomes manifest with a large number of elec-

trodes. Thus, real head shape models are definitely needed. For this purpose, we are currently measuring with a precision of a few millimeters the locations of the electrodes on the scalp with a 3D-localization device (ISOTRAK by Polhemus Inc., Colchester, VT, USA). This electrode localization system avoids the errors introduced from assuming equal distances between electrodes and it allows the modeling of the real head shape. A spherical model, as used in the examples presented here, is certainly only a crude approximation.

In addition to the real head shape, the solution space can be restricted to the real brain space by using the information derived from MRI images of the subjects. We believe that a combination with other imaging modalities is crucial to increase the spatial resolution of the method.

Another point concerns the inappropriateness

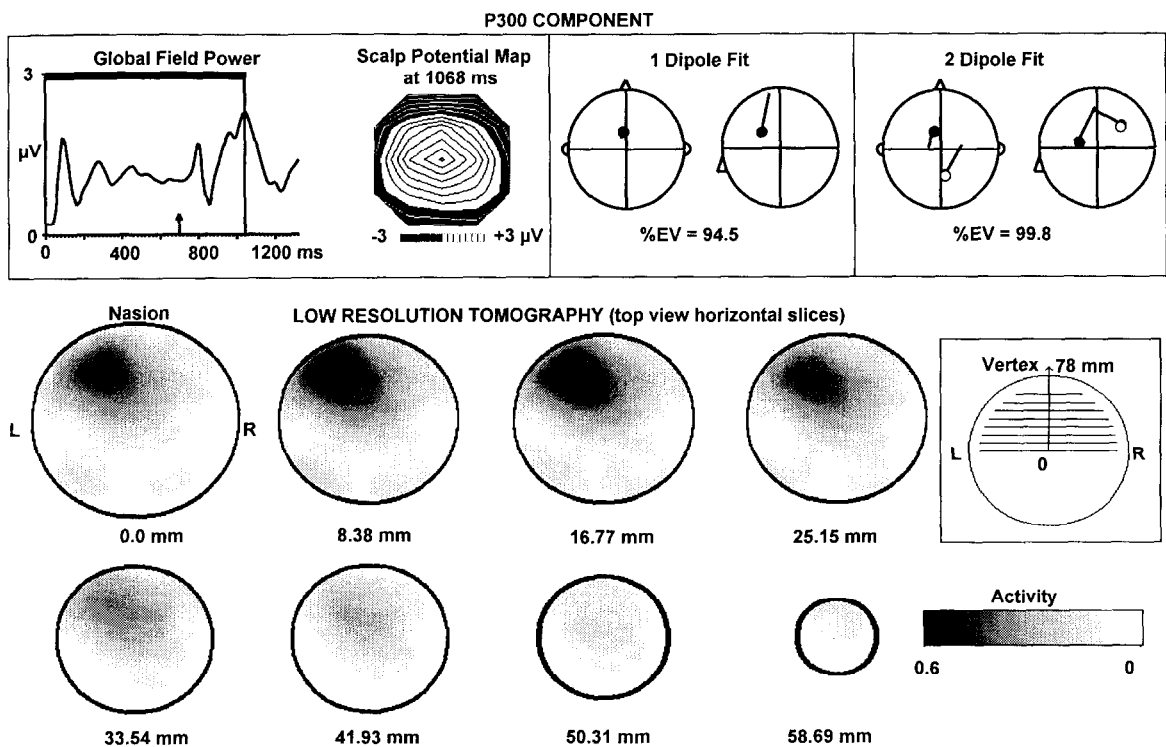


Fig. 9. Low resolution brain electromagnetic tomographic (LORETA) images (shown with the same conventions as in Fig. 7) corresponding to the P300 component after the visual target stimulus, indicated as a small arrow at 704 ms in the Global Field Power curve. The LORETA images suggest strong left frontal activity, while the one and two dipole models produce deep midline generators.

of analyzing the signals averaged over subjects, since different head-brain shapes and intra-individual functional differences are averaged. The last point is especially true for cognitive components. Thus, the correct strategy would be to localize the activities for each individual subject separately (using exact electrode positions and the individual real head shape information), and averaging the LORETA solutions when the mean over subjects is desired. Due to the large amount of data and of computation time required, this has not been done in the present introductory paper.

From a methodological point of view, the selection of GFP peaks in grand mean ERPs is certainly a grossly simplified ERP analysis technique. A more appropriate strategy would be to perform a temporal segmentation based on spatial properties of the field in order to find the functional microstates that correspond to the functional information processing steps. Such segmentation strategies have been presented repeatedly (Lehmann, 1987; Brandeis and Lehmann, 1989; Michel et al., 1992; Michel and Lehmann, 1993). This would result in a reduction of the number of ERP maps to analyze. The localization of the sources of the functional microstate maps would finally result in a limited number of different brain activity distributions, each reflecting a certain information processing step.

In summary, many improvements are necessary to take full advantage of the localization strategy presented here. All of these points are, however, also true for the other localization strategies presented up to now. Our method does not create new methodological problems but it clearly exposes those that were always present in the localization procedures and on which many groups are currently working. We are convinced that our method in combination with modern multimodal imaging strategies will bring new insight into functional brain processes.

Appendix

The 3D inverse solution derived here corresponds to the “smoothest” current density capa-

ble of explaining the measured data. Formally, for noise-free instantaneous measurements, the discrete problem is:

$$\min_{\mathbf{J}} \|\mathbf{B} \mathbf{W} \mathbf{J}\|^2, \text{ under constraint: } \Phi = \mathbf{K} \mathbf{J} \quad (1)$$

where Φ is a N -vector comprised of measurements (EEG and/or MEG); $\mathbf{J} = (\mathbf{j}_1^T, \mathbf{j}_2^T, \dots, \mathbf{j}_M^T)^T$ is a $3M$ -vector comprised of the current densities \mathbf{j} (3-vector) at M points with known locations within the brain volume; \mathbf{K} is a transfer $N \cdot 3M$ -matrix with α -th row $(\mathbf{k}_{\alpha 1}^T, \mathbf{k}_{\alpha 2}^T, \dots, \mathbf{k}_{\alpha M}^T)$, where \mathbf{k} is the lead field (3-vector), which can be either electric or magnetic depending on the nature of the α -th measurement (see Pascual-Marqui and Biscay-Lirio (1993), Eqs. (2) and (3) therein, as particular examples for the radial magnetic component and the electric potential in a simple head model); \mathbf{W} is a diagonal $3M \cdot 3M$ -matrix with $w_{ii} = \|\mathbf{K}_i\|$, where \mathbf{K}_i is the i -th column of \mathbf{K} ; and \mathbf{B} is the discrete Laplacian operator $3M \cdot 3M$ -matrix. Specifically, let $\mathbf{Z} = \mathbf{W} \mathbf{J} = (\mathbf{z}_1^T, \mathbf{z}_2^T, \dots, \mathbf{z}_M^T)^T$, where \mathbf{z} (3-vector) is the weighted current density, and let $\mathbf{B} \mathbf{Z} = (\mathbf{l}_1^T, \mathbf{l}_2^T, \dots, \mathbf{l}_M^T)^T$ be the corresponding discrete Laplacian. Then for a regular cubic grid of points (with minimum inter-point distance d) confined to the brain volume, the matrix \mathbf{B} is such that:

$$\mathbf{l}_i = \frac{1}{d^2} \left(6\mathbf{z}_i - \sum_p \mathbf{z}_p \right),$$

$$\forall p \text{ under constraint: } \|\mathbf{r}_i - \mathbf{r}_p\| = d \quad (2)$$

where \mathbf{r}_i denotes the position vector of the i -th grid point. With this definition, matrix \mathbf{B} is symmetric, non-singular, and sparse.

For a dense grid ($M \gg N$), if \mathbf{W} is non-singular, the unique solution to (1) can be shown to be (Rao and Mitra, 1983):

$$\hat{\mathbf{J}} = \mathbf{T} \Phi,$$

$$\text{with: } \mathbf{T} = (\mathbf{W} \mathbf{B}^T \mathbf{B} \mathbf{W})^{-1} \mathbf{K}^T$$

$$\times \left\{ \mathbf{K} (\mathbf{W} \mathbf{B}^T \mathbf{B} \mathbf{W})^{-1} \mathbf{K}^T \right\}^+ \quad (3)$$

where \mathbf{A}^+ denotes the Moore-Penrose pseudoinverse of matrix \mathbf{A} . The estimated 3D distribution of the electrically active neural tissue is given by $\hat{\mathbf{J}}$.

The discrete nature of formulation (1)–(3) was

chosen for practical reasons, although in principle, the continuous version ($M \rightarrow \infty$) could have been treated as well. The inverse solution (3) is presented for electric and magnetic measurements, performed either separately or simultaneously. Furthermore, the solution can be applied to any physical head model, with arbitrary geometry and conductivity properties, as long as the appropriate equations for the lead field (matrix \mathbf{K} in (1) and (3)) are available.

The classical forward problem is represented in (1) as the constraint. When rewritten as $\Phi = (\mathbf{K}\mathbf{W}^{-1})(\mathbf{W}\mathbf{J})$, it becomes clear that the role of the matrix \mathbf{W} is to express the measurements as an expansion in terms of normalized basis functions, which are precisely the columns of $(\mathbf{K}\mathbf{W}^{-1})$. In this way, all discrete current densities are actually given equal weight regardless of location.

Minimization of the total squared Laplacian (1) is a common choice in generalized signal processing for maximizing smoothness (see e.g. Titterton, 1985). Under this condition, the solution corresponding to a single point source is a smeared or blurred version of the point, even in 3D space.

Anatomical and physiological a priori knowledge can be embodied in the inverse solution by means of constraints. In general, the higher the amount of a priori information, the higher the resolution of the tomography. For example, if it can be assured that the measurements are due to generators distributed exclusively on the cortex, and if the exact geometry of the cortex is known, then for a grid confined to this surface, and with an appropriately defined discrete surface Laplacian (modification of Eq. (2)), Eqs. (1) and (3) hold.

At present, two main lines of research are in progress. In one, detailed quantitative properties of the inverse solution are evaluated, such as localization error and dispersion as functions of source characteristics, number of measurements, measurement noise, and amount of a priori physiological and anatomical information. In the second, measurement and biological noise sources are dealt with explicitly, and the method is extended to time varying data in the time and in the frequency domains.

Acknowledgments

This research was in part supported by the Swiss National Science Foundation, grant No. 32-39420.93, and a Roche Research Foundation Grant. The authors are very grateful to Prof. T. Landis for encouragement, support, and fruitful discussions.

References

- Andersen, P. and Andersson, S.A. (1968) *Physiological Basis of the Alpha Rhythm*, Appleton-Century-Crofts, New York.
- Ary, J.P., Klein, S.A. and Fender, D.H. (1981) Location of sources of evoked scalp potentials: corrections of skull and scalp thickness. *IEEE Trans. Biomed. Eng.*, 28: 447–452.
- Barrett, G., Blumhardt, L., Halliday, A.M., Halliday, E. and Kriss, A. (1976) A paradox in the lateralization of the visual evoked response. *Nature*, 261: 253–255.
- Başar-Eroglu, C., Schmielau, F., Schramm, U. and Schult, J. (1991) P300 response of hippocampus analyzed by means of multielectrodes in cats. *Int. J. Neurosci.*, 60: 239–248.
- Bland, B.H. (1986) The physiology and pharmacology of hippocampal formation theta rhythms. *Progr. Neurobiol.*, 26: 1–54.
- Bland, B.H. and Colom, L.V. (1993) Extrinsic and intrinsic properties underlying oscillation and synchrony in limbic cortex. *Progr. Neurobiol.*, 41: 157–208.
- Brandeis, D. and Lehmann, D. (1989) Segments of ERP map series reveal landscape changes with visual attention and subjective contours. *Electroenceph. Clin. Neurophysiol.*, 73: 507–519.
- Brown, W.S., Larson, E.B. and Jeeves, A. (1994) Directional asymmetries in interhemispheric transmission time: evidence from visual evoked potentials. *Neuropsychologia*, 32: 439–448.
- Capaul, M. (1990) Human brain potential maps visually evoked by hemiretinal stimulations. Doctoral Dissertation, Faculty of Medicine, University of Zurich, Zurich.
- Darcey, T.M., Ary, J.P. and Fender, D.H. (1980) Spatio-temporal visually evoked scalp potentials in response to partial-field patterned stimulation. *Electroenceph. Clin. Neurophysiol.*, 50: 348–355.
- Eckhorn, R. and Reitboeck, H.J. (1989) Stimulus-specific synchronization in cat visual cortex and their possible role in visual pattern recognition. In: H. Haken (Ed.), *Synergetics of Cognition*, Springer Series in Synergetics, Springer-Verlag, Berlin, pp. 1–14.
- Elbert, T., Rockstroh, B., Hampson, S., Pantev, C. and Hoke, M. (1994) The magnetic counterpart of the contingent negative variation. *Electroenceph. Clin. Neurophysiol.*, 92: 262–272.
- Engel, A.K., König, P., Gray, C.M. and Singer, W. (1990)

- Stimulus-dependent neuronal oscillations in cat visual cortex: intercolumnar interaction as determined by cross-correlation analysis. *Eur. J. Neurosci.*, 2: 588–608.
- Fender, D.H. (1987) Source localization of brain electrical activity. In: A.S. Gevins and A. Rémond (Eds.), *Handbook of Electroencephalography and Clinical Neurophysiology, Rev. Ser., Vol.1: Methods of Analysis of Brain Electrical and Magnetic Signals*, Elsevier, Amsterdam, pp. 355–399.
- Ford, M.R., Sidman, R.D. and Ramsey, G. (1993) Spatio-temporal progression of the AEP P300 component using the cortical imaging technique. *Brain Topogr.*, 6: 43–50.
- Gray, C.M., König P., Engel, A.K. and Singer, W. (1989) Oscillatory responses in cat visual cortex exhibit inter-columnar synchronization which reflects global stimulus patterns. *Nature*, 338: 334–337.
- Grüsser, O.-J. and Landis, T. (1991) *Visual Agnosia and other Disturbances of Visual Perception and Cognition: Vision and Visual Disfunction*, Vol. 12, Macmillan Press, London.
- Hämäläinen, M.S. and Sarvas, J. (1989) Realistic conductivity geometry model of the human head for interpretation of neuromagnetic data. *IEEE Trans. Biomed. Eng.*, 36: 165–171.
- Harvey, A.R. (1980) A physiological analysis of subcortical and commissural projections of areas 17 and 18 of the cat. *J. Physiol.*, 302: 507–534.
- Henderson, C.J., Butler, S.R. and Glass, A. (1975) The localization of equivalent dipoles of EEG sources by the application of electrical field theory. *Electroenceph. Clin. Neurophysiol.*, 39: 117–130.
- Ilmoniemi, R.J. (1993) Models of source currents in the brain. *Brain Topogr.*, 5: 331–336.
- Ioannides, A.A., Bolton, J.P.R. and Clarke, C.J.S. (1990) Continuous probabilistic solutions to the biomagnetic inverse problem. *Inverse Problems*, 6: 523–542.
- Johnson, R., Jr. (1993) On the neural generators of the P300 component of the event related potential. *Psychophysiology*, 30: 90–97.
- Kavanagh, R.N., Darcey, T.M., Lehmann, D. and Fender, D.H. (1978) Evaluation of methods for three-dimensional localization of electrical sources in the human brain. *IEEE Trans. Biomed. Eng.*, 25: 421–429.
- Kiss, I., Dashieff, R.M. and Lordeon, P. (1989) A parieto-occipital generator for P300: evidence from human intracranial recordings. *Int. J. Neurosci.*, 49: 133–139.
- Kreiter, A.K. and Singer, W. (1992) Oscillatory neuronal responses in the visual cortex of the awake macaque monkey. *Eur. J. Neurosci.*, 4: 369–375.
- Lehmann, D. (1987) Principles of spatial analysis. In: A.S. Gevins and A. Rémond (Eds.), *Handbook of Electroencephalography and Clinical Neurophysiology, Rev. Ser., Vol.1: Methods of Analysis of Brain Electrical and Magnetic Signals*, Elsevier, Amsterdam, pp. 309–354.
- Lehmann, D. and Skrandies, W. (1979) Multichannel evoked potential fields show different properties of human upper and lower hemiretina systems. *Exp. Brain Res.*, 35: 151–159.
- Lehmann, D. and Skrandies, W. (1980) Reference-free identification of components of checkerboard-evoked multichannel potential fields. *Electroenceph. Clin. Neurophysiol.*, 48: 609–621.
- Lehmann, D., Darcey, T.M. and Skrandies, W. (1982). Intracerebral and scalp fields evoked by hemiretinal checkerboard reversal, and modeling of their dipole generators. In: J. Courjon, F. Maugière and M. Revol (Eds.), *Clinical Applications of Evoked Potentials in Neurology*, Raven Press, New York, pp. 41–48.
- Llinas, R.R. (1988) The intrinsic electrophysiological properties of mammalian neurons: insights into central nervous system function. *Science*, 242: 1654–1664.
- Michel, C.M. and Lehmann, D. (1993) Single doses of piracetam affect 42-channel event related potential microstate maps in a cognitive paradigm. *Neuropsychobiology*, 28: 212–221.
- Michel, C.M., Henggeler, B. and Lehmann, D. (1992) 42-channel potential map series to visual contrast and stereo stimuli: perceptual and cognitive event related segments. *Int. J. Psychophysiol.*, 12: 133–145.
- Murthy, V.N. and Tetz, E.E. (1991) Synchronized 25–35 Hz oscillations in sensorimotor cortex of awake monkeys. *Soc. Neurosci. Abstr.*, 17: 310.
- O'Connor, T.A. and Starr, A. (1985) Intracranial potentials correlated with an event related potential, P300, in cat. *Brain Res.*, 339: 27–38.
- Okada, Y.C., Kaufman, L. and Williamson, S.J. (1983) The hippocampal formation as a source of the slow endogenous potentials. *Electroenceph. Clin. Neurophysiol.*, 55: 417–426.
- Pantev, C., Hoke, M., Lehnertz, K., Luetkenhoener, B., Anogianakis, G. and Wittkowski, W. (1988) Tonotopic organization of the human auditory cortex revealed by transient auditory magnetic fields. *Electroenceph. Clin. Neurophysiol.*, 69, 160–170.
- Pascual-Marqui, R.D. and Biscay-Lirio, R. (1993) Spatial resolution of neuronal generators based on EEG and MEG measurements. *Int. J. Neurosci.*, 68: 93–105.
- Rao, C.R. and Mitra, S.K. (1973) Theory and application of constrained inverse of matrices. *SIAM J. Appl. Math.*, 24: 473–488.
- Scherg, M. and Berg, P. (1991) Use of a prior knowledge in brain electromagnetic source analysis. *Brain Topogr.*, 4: 143–151.
- Scherg, M., Vajsar, J. and Picton, T.W. (1989) A source analysis of the late human auditory evoked potentials. *J. Cogn. Neurosci.*, 1: 336–355.
- Silva, L.R., Amitai, Y. and Connors, B.W. (1991) Intrinsic oscillations of neocortex generated by layer 5 pyramidal neurons. *Science*, 251: 432–435.
- Skrandies, W. (1987) The upper and lower visual field of man: electrophysiological and functional differences. *Progr. Sensory Physiol.*, 8: 1–93.
- Skrandies, W., Richter, M. and Lehmann, D. (1980) Checkerboard-evoked potentials: topography and latency for onset, offset, and reversal. In: H.H. Kornhuber and L. Deecke

- (Eds.), *Motivation, Motor, and Sensory Processes of the Brain*, Progress in Brain Research, Vol. 54, Elsevier, Amsterdam, pp. 227–250.
- Steriade, M., Gloor, P., Llinas, R.R., Lopes da Silva, F.H. and Mesulam, M.M. (1990) Basic mechanisms of cerebral rhythmic activities. *Electroenceph. Clin. Neurophysiol.*, 76: 481–508.
- Titterton, T.M. (1985) Common structure of smoothing techniques in statistics. *Int. Stat. Rev.*, 53: 141–170.
- Trahms, L., Erné, S.N., Stehr, R., Seibert, E. and Friederici, A. (1993) Multichannel magnetic recording of P300 activity. *Physiol. Measurement*, 14: A85–A89.
- Wang, J.Z., Williamson, S.J. and Kaufman, L. (1992) Magnetic source images determined by a lead-field analysis: the unique minimum-norm least-squares estimation. *IEEE Trans. Biomed. Eng.*, 39: 665–675.
- Wikwo, J.P., Jr., Gevins, A. and Williamson, S.J. (1993) The future of the EEG and MEG. *Electroenceph. Clin. Neurophysiol.*, 87: 1–9.
- Williamson, S.J. and Kaufman, L. (1987) Analysis of neuro-magnetic signals. In: A.S. Gevins and A. Rémond (Eds.), *Handbook of Electroencephalography and Clinical Neurophysiology*, Rev. Ser., Vol. 1: Methods of Analysis of Brain Electrical and Magnetic Signals, Elsevier, Amsterdam, pp. 405–488.
- Witte, H., Lehmann, D., Capaul, M. and Rother, M. (1992) Application of instantaneous frequency maps for quantification of visual evoked potentials. *Automedica*, 14: 133–143.